Excess open solar magnetic flux from satellite data: 2. A survey of kinematic effects

JOURNAL OF GEOPHYSICAL RESEARCH, VOL. 114, A11104, doi:10.1029/2009JA014450, 2009

Excess open solar magnetic flux from satellite data: 2. A survey of kinematic effects

M. Lockwood,[1,2] M. Owens,[3] and A. P. Rouillard[1,2]

Received 12 May 2009; accepted 22 July 2009; published 12 November 2009.

[1] We investigate the "flux excess" effect, whereby open solar flux estimates from spacecraft increase with increasing heliocentric distance. We analyze the kinematic effect on these open solar flux estimates of large-scale longitudinal structure in the solar wind flow, with particular emphasis on correcting estimates made using data from near-Earth satellites. We show that scatter, but no net bias, is introduced by the kinematic "bunching effect" on sampling and that this is true for both compression and rarefaction regions. The observed flux excesses, as a function of heliocentric distance, are shown to be consistent with open solar flux estimates from solar magnetograms made using the potential field source surface method and are well explained by the kinematic effect of solar wind speed variations on the frozen-in heliospheric field. Applying this kinematic correction to the Omni-2 interplanetary data set shows that the open solar flux at solar minimum fell from an annual mean of 3.82×10^{16} Wb in 1987 to close to half that value (1.98×10^{16} Wb) in 2007, making the fall in the minimum value over the last two solar cycles considerably faster than the rise inferred from geomagnetic activity observations over four solar cycles in the first half of the 20th century.

Citation: Lockwood, M., M. Owens, and A. P. Rouillard (2009), Excess open solar magnetic flux from satellite data: 2. A survey of kinematic effects, *J. Geophys. Res.*, *114*, A11104, doi:10.1029/2009JA014450.

1. Introduction

[2] In our companion paper [*Lockwood et al.*, 2009] (hereinafter referred to as paper 1), we discussed the Ulysses result of the latitudinal invariance of the radial heliospheric field and its relationship to the "flux excess" detected by *Owens et al.* [2008a]. As given in paper 1, using the latitudinal invariance gives the signed open flux (of one polarity), F_S to be

$$F_S = 2\pi r^2 \langle |B_r|_T \rangle_{CR} \quad (1)$$

where r is the heliospheric distance and B_r is the radial component of the heliospheric field. The subscript CR is to denote that the averages are taken over a Carrington Rotation interval (or alternatively a Bartels rotation interval) to remove longitudinal structure. T is the timescale on which B_r data are preaveraged and then converted into absolute values. *Lockwood et al.* [2004] showed that the error introduced into F_S by use of equation (1) was <5% if averages over a 27 days or longer are taken: this was shown to be true for both solar maximum and solar minimum conditions.

[3] Recently *Owens et al.* [2008a] have studied the open solar flux (in fact, they studied the unsigned flux; i.e., $2F_S$) deduced from spacecraft in different parts of the heliosphere using $T = 1$ h. They find considerable agreement between the data sequences from different craft which gives strong support to the use of equation (1). However, although they find that neither latitudinal nor longitudinal separation of the craft introduced significant differences on average, they did find a consistent increase in the estimated F_S with heliocentric distance r, which became especially pronounced at above about 2.5 AU. This "flux excess" effect was discussed in relation to the third Ulysses perihelion pass in paper 1. Although the survey by *Owens et al.* [2008a] did not find a consistent variation of the excess flux with heliographic latitude Λ, these authors noted that any variation with Λ in Ulysses data was convolved with the dependence on r owing to the nature of the satellite's orbit. In fact, these data are further complicated by the sunspot cycle phase ε which changes on timescales comparable to the Ulysses orbital period; separation of the effects of r, Λ and ε are presented by *Lockwood and Owens* [2009]. In paper 1 we report a difference between the excess flux in the streamer belt and the large polar coronal holes for the third pass of Ulysses which was near solar minimum.

[4] The open solar flux (here defined as the flux threading the coronal source surface) has also been evaluated from solar magnetograms using the potential field source surface (PFSS) method [e.g., *Schatten et al.*, 1969; *Altschuler and Newkirk*, 1969; *Schatten*, 1999]. In this method, the observed photospheric magnetic fields from a magnetogram

[1]Space Environment Physics, School of Physics and Astronomy, Southampton University, Southampton, UK.
[2]Also at Space Science and Technology Department, Rutherford Appleton Laboratory, Chilton, UK.
[3]Space and Atmospheric Physics Group, Blackett Laboratory, Imperial College London, London, UK.

0148-0227/09/2009JA014450$09.00

are mapped through the solar corona to the source surface (assumed to be spherical with radius $r = r_o = 2.5$ solar radii = (2.5/251)AU, where 1 AU $\approx 1.5 \times 10^{11}$ m) with a number of assumptions. Agreement with data from in situ observations of the heliospheric field has generally been good [*Wang and Sheeley*, 2003], but two caveats to this comparison should be noted. First, the magnetogram data require processing using a latitude-dependent instrument saturation factor [*Wang and Sheeley*, 1995] which has been the subject of some debate [*Svalgaard et al.*, 1978; *Ulrich*, 1992]. Second, for the satellite data taken near Earth (at heliocentric distance $r \approx 1$ AU), preaveraging of B_r on timescales of $T = 1-2$ days (before absolute values are taken) has been required: otherwise the latter would show a flux excess (relative to the PFSS values). As discussed in paper 1, the idea is that the value of T is chosen so that it is not so large that the opposing field in "toward" and "away" interplanetary sectors of the source field are canceled (which would cause the true open solar flux to be underestimated) but should be large enough that small-scale structure generated in the heliosphere (which does not reflect structure in the source field and so would cause the true open flux to be overestimated) is averaged out. Increasing T results in lower F_S values given by equation (1) [*Lockwood et al.*, 2006], but there is no a priori reason for adopting any one value of T. At any one time, there will always be a T for which the near-Earth estimate using equation (1) will equal the true coronal source flux, but without an understanding of how to compute it, we cannot be sure of the correct T to use nor if it is constant with either time or heliographic coordinates. Indeed, it may be that the heliospheric effects cannot be separated from source sector structure by their timescales, in which case the use of T has no physical justification at all. A value for T of 1 day has commonly been adopted because it has given a good general match of the variations in F_S deduced from near-Earth in situ data to those from the PFSS method [*Wang and Sheeley*, 1995; *Wang et al.*, 2000; *Lockwood et al.*, 2006].

[5] Paper 1 analyzed the effect of various T, and of plasma time-of-flight associated with large-scale longitudinal solar wind variability ("kinematic effects"; see section 2), on the flux excess detected by comparison of data from the near-Earth ACE satellite with that from the Ulysses spacecraft during its third perihelion pass. Paper 1 found that both effects provided a partial allowance for the flux excess, although the kinematic correction performed more satisfactorily in a number of respects. However, it also showed that these are not equivalent corrections in that the kinematic correction is allowing for larger-scale structure in the heliosphere (giving variations at any one point on timescales 1–27 days) whereas the averaging timescale can only make allowance for smaller-scale structure (on timescales of $T \leq 1$ day). Furthermore, paper 1 showed that structure on timescales $T < 1$ h was not contributing to the observed flux excess because its effect was the same at all r and Λ. The averaging and the kinematic corrections generated somewhat different estimates of the open solar flux F_S. The kinematic correction gave a more uniform variation of the radial field with latitude and gave closer agreement between the ACE and Ulysses data (but not by an overwhelmingly large factor). One major advantage of the kinematic correction was that it matched a difference between the streamer belt and the sunspot-minimum polar coronal hole, whereas averaging over a fixed time interval T did not. In the present paper, we consider the kinematic correction of coronal source flux estimates from r near 1 AU and elsewhere in the heliosphere and show it to be consistent, not only with the flux excess variation as a function of r in the inner heliosphere as deduced by *Owens et al.* [2008a], but also with PFSS open flux estimates.

2. Theory of Kinematic Effects

[6] Figure 1 is a schematic of how large-scale temporal (Figures 1a–1c) and spatial (Figures 1d–1f) structure in the radial solar wind flow speed can give rise to excess flux via purely kinematic (time-of-flight) effects and how this excess flux grows with heliocentric distance r. In both cases, this arises because the field becomes distorted as it is frozen into the longitudinally variable flow. Both spatial and temporal effects result in the excess flux in measurements made at $r \approx r_1 = 1$ AU which therefore need correcting for these kinematic effects. As suggested by comparison of Figures 1c and 1f, it will not be easy to distinguish the spatial and temporal effects in many cases, as both result in an amplification of the magnitude of the ambient radial field in regions of increasing solar wind speed V ($dV > 0$) and a reduction (and, at sufficiently large r, a reversal in polarity) in regions of decreasing solar wind speed ($dV < 0$). Examples of such kinematic effects have been reported in the streamer belt: *Riley and Gosling* [2007] have shown that events of near-radial IMF reported by *Jones et al.* [1998] are explained by the kinematic effect in rarefaction regions where the solar wind velocity decays ($dV < 0$). *Burlaga and Barouch* [1976] provided equations which quantify the effects shown schematically in Figure 1. It is important to note that these equations do not allow for dynamical stream–stream interactions that will inevitably accompany the kinematic effects associated with increasing solar wind flow speeds in compression regions ($dV > 0$) [*Gosling*, 1996; *Gosling and Pizzo*, 1999; *Arge and Pizzo*, 2000]. Compression regions steepen as they propagate to greater r, until shocks form. However, the lack of dynamical effects in rarefaction regions means that the kinematic effects will grow with increasing r until the IMF becomes radial [*Jones et al.*, 1998; *Riley and Gosling*, 2007].

[7] *Burlaga and Barouch* [1976, equation (16)] gives the vector field at a heliocentric distance r for purely kinematic effects:

$$\underline{\boldsymbol{B}} = \left\{(r_o/r)^2 B_{ro} + \Delta B_r\right\}\underline{\boldsymbol{r}} + \mu B_{\varphi o}(r_o/r)\varphi \qquad (2)$$

where

$$\Delta B_r = [\partial V/\partial t]_o \frac{\mu(r - r_o)}{\Omega r_o V \cos\lambda}(r_o/r)^2 B_{\varphi o} \qquad (3)$$

B_{ro} and $B_{\varphi o}$ are the radial and longitudinal components of the field at the coronal source surface $r = r_o$, λ is the heliographic latitude, Ω is the angular rotation velocity of the solar atmosphere, V is the (radial) solar wind speed and μ is a dimensionless parameter that allows for the kinematic steepening of gradients owing to time-of-flight effects: it

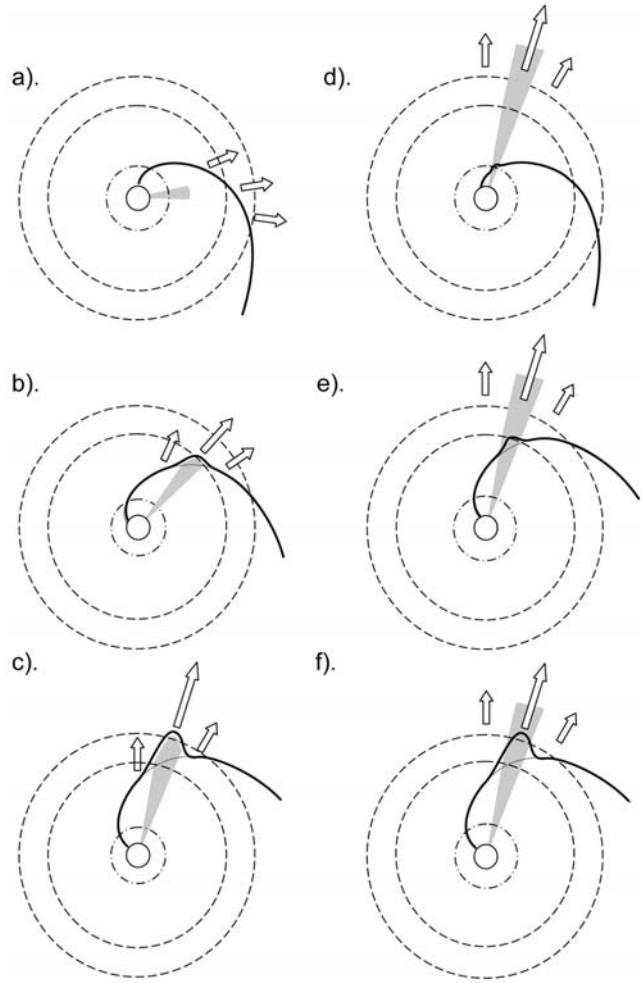

Figure 1. Schematic of the evolution of an interplanetary field line for (a–c) a transient flow speed increase and (d–f) a long-lived rotating fast flow region threaded by a seed tangential field. In both cases the fast flow region is shaded and the growing distortion of the field line (with respect to a Parker spiral shown by the dotted line) makes an additional contribution to the mean radial field (which averaged over a full Bartels rotation is $\langle|\Delta B_r|\rangle_{27}$), and this additional contribution grows with increasing heliocentric distance r.

therefore depends on r. $[\partial V/\partial t]_o$ is the temporal solar wind velocity gradient at $r = r_o$. Equation (3) is also readily derived by applying the frozen-in theorem to two plasma elements on the same field line but on solar wind streamlines of different speed. As pointed out by Burlaga and Barouch, for uniform solar wind speed $[\partial V/\partial t]_o = 0$, this equation reduces to the standard Parker spiral equation. Note that the "seed" tangential field $B_{\varphi o}$ is a constant for a given field line. From equation (2) the magnitude of the $\underline{\boldsymbol{\varphi}}$ component at general r is

$$B_{\varphi r} = \mu B_{\varphi o}(r_o/r) \tag{4}$$

Substituting (4) and (3) gives

$$\Delta B_r = [\partial V/\partial t]_o \frac{(1 - r_o/r)}{\Omega V \cos\lambda} B_{\varphi r} \tag{5}$$

If we consider initially only kinematic effects; that is, with no modification of the solar wind velocity vector $\boldsymbol{V}$ by stream–stream interactions, the radial velocities V and $V + dV$ observed at r (at times t and dt) will be the same for those plasma parcels at all r. Plasma parcels seen dt apart at r will have left the coronal source surface at an interval dt_o apart. Defining the times-of-flight for the radial velocities V and $V + dV$ to be τ_V and τ_{V+dV}:

$$dt_o = dt + \tau_V - \tau_{V+dV} = dt + \{(r - r_o)/V\} - \{(r - r_o)/(V + dV)\} \tag{6}$$

Thus $[\partial V/\partial t]_o = dV/dt_o$ can be computed as all the terms on the right-hand side of equation (5) are known from the spacecraft data at r. Hence ΔB_r can be predicted from solar wind and IMF observations at r (for the kinematic assumption of constant V). The gray histogram in Figure 2 shows the distribution of ΔB_r values computed using equations (5) and (6) from hourly observations taken near Earth ($r = r_1 = 1$ AU) between 1963 and 2008 as compiled in the Omni-2 data set of hourly interplanetary averages (the continuation of the work of *Couzens and King* [1986]).

[8] In compression regions where solar wind speeds increase at any one latitude ($dV > 0$), dynamical stream–stream interaction regions form on the leading boundaries of coronal holes [*Cranmer*, 2002] where fast wind catches up with slow wind ahead of it and the assumption of constant V becomes invalid. These flow gradients steepen as they propagate outward but do not generally form shocks until $r \approx 2$ AU [e.g., *Gosling*, 1996]. Such interaction regions at $r = 1$ AU typically last on the order of 1 day [e.g., *Gosling and Pizzo*, 1999]. To remove their effect on the kinematic correction, we here use smoothed values of V: daily means in dV are interpolated to apply at the centers of the hourly averaging intervals of the IMF data. The smoothing time constant of 1 day represents a compromise: it smoothes out much of the dynamical effects in interaction regions, but the overall autocorrelation function of the solar wind speed at 1 AU falls to 0.5 for lags near 30 h [*Lockwood*, 2002], hence using intervals any longer than 1 day would cause us to also average out considerable larger-scale longitudinal structure in the source solar wind speed. The use of 1 day smoothing means that we are predicting the kinematic effects of flow speed structure on timescales of 1–27 days. The effectiveness of this procedure to remove dynamic interaction effects in compression regions is discussed later in section 2.

[9] From equation (6), *Burlaga and Barouch* [1976] show that the parameter μ is given by

$$\mu = \{1 - (r - r_o)[\partial V/\partial t]_o/V^2\}^{-1} \tag{7}$$

Hence computation of μ as a function of r requires knowledge of the ratio $[\partial V/\partial t]_o/V^2$. This ratio is shown in Figure 3 for the same data set as Figure 2. Positive values are compression regions ($[\partial V/\partial t]_o > 0$) which give $dt < dt_o$, negative values are rarefaction regions ($[\partial V/\partial t]_o < 0$) which give $dt > dt_o$. Note that V values have been given in units of AU s^{-1} as this gives ready application with r values expressed in units of AU.

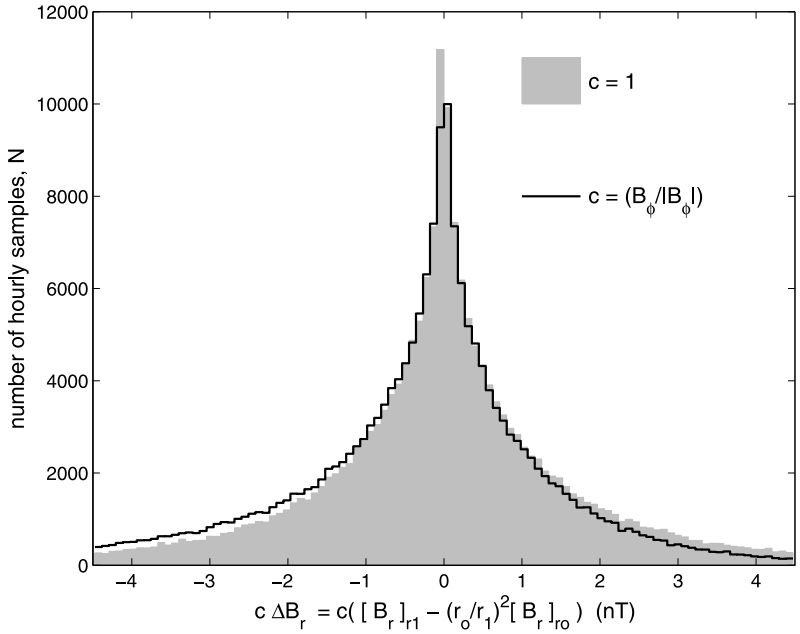

Figure 2. The distribution of predicted radial field difference (normalized to $r = r_1 = 1$AU) $c \times \Delta B_{r1} = c \times \{[B_r]_{r1} - (r_0/r_1)^2[B_r]_{ro}\}$ between $r_1 = 1$AU and the coronal source surface at $r_o = 2.5/251$ AU. The shaded area is for $c = 1$ (and so includes the effect of the polarity of B_φ), and the black line is for $c = B_\varphi/|B_\varphi|$ (i.e., $c = \pm 1$) which removes the effect of the polarity of B_φ. The plot is for hourly data from the entire Omni-2 data set for 1963–2008.

[10] Studying equations (4) and (7) highlights the limitations of this theory in compression regions. At sufficiently large r, $\{(r - r_o)\ [\partial V/\partial t]_o/V^2\}$ rises to unity for $[\partial V/\partial t]_o > 0$ and hence, by (7), μ becomes infinite and, by (4), so does $B_{\varphi r}$.

[11] Equation (5) shows that for a fixed r and λ, the ratio of $\{[\partial V/\partial t]_o/V^2\}/\Delta B_r$ depends on $(VB_{\varphi r})$. For a positive/negative $B_{\varphi r}$, a given polarity of $[\partial V/\partial t]_o$ will give the same/opposite polarity of ΔB_r, respectively. To remove the dependence on the polarity of $B_{\varphi r}$, we here

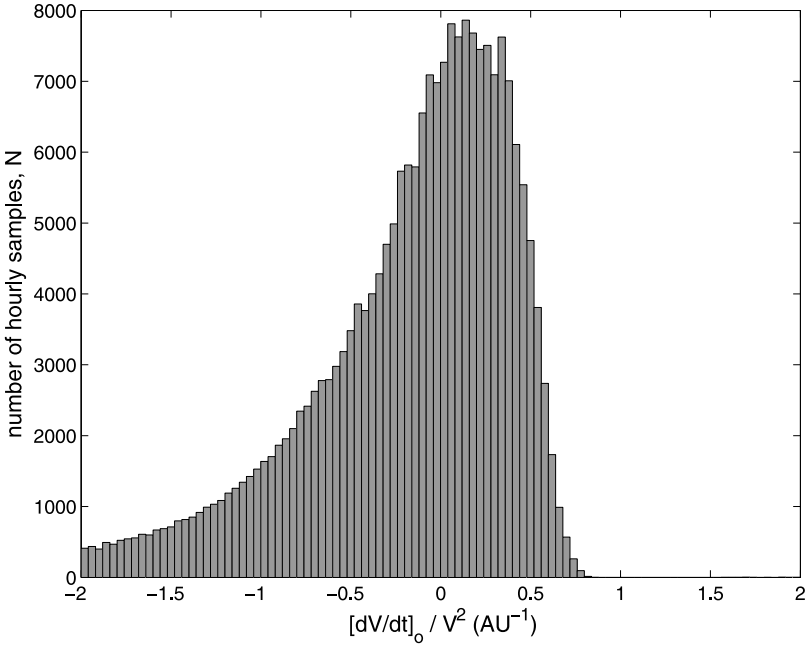

Figure 3. The distribution of predicted values at $r = r_o$ of the ratio $[\partial V/\partial t]_o/V^2$ (with V here expressed in units of AU s^{-1}). The ∂V values are interpolated from daily means to remove effects of fine structure in the variation in V. The plot shows the hourly values from the entire Omni-2 data set for 1963–2008. Positive/negative values are for compression/rarefaction regions, respectively.

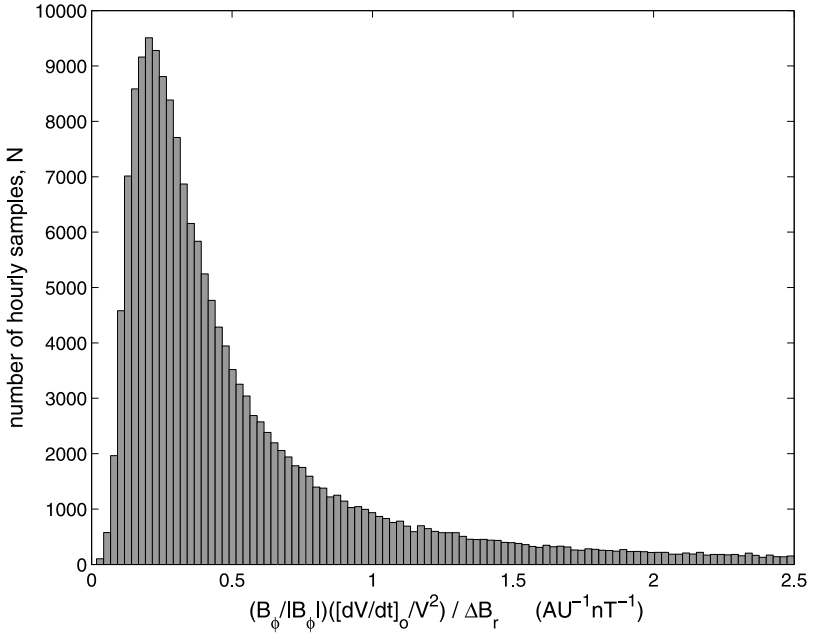

Figure 4. The distribution of predicted values of the factor $c\{[\partial V/\partial t]_o/V^2\}/\Delta B$r (with V expressed in units of AU s^{-1}). The ∂V values are as used in Figure 3. The term $c = B_\varphi/|B_\varphi| = \pm 1$ removes the effect of the polarity of B_φ. The plot shows the hourly values from the entire Omni-2 data set for 1963–2008. The mode value is 0.2, and this distribution includes both compression ($[\partial V/\partial t]_o > 0$, $\Delta B r/c > 0$) and rarefaction ($[\partial V/\partial t]_o < 0$, $\Delta B r/c < 0$) regions.

use $c = B_{\varphi r}/|B_{\varphi r}| = \pm 1$. Figure 4 shows the distribution of values of $c\{[\partial V/\partial t]_o/V^2\}/\Delta B_r$ from the same data set as in Figures 2 and 3. The mode value of 0.02 applies to both compression and rarefaction regions.

[12] As in paper 1, we define the signed flux deficit for measurements made at r and r_1 to be

$$\Delta F_S(r) = 2\pi\{|B_r|r^2 - |B_{r1}|r_1^2\} \quad (8)$$

The radial term of equation (2) gives $B_r = (r_o/r)^2 B_{ro} + \Delta B_r$ and $B_{r1} = (r_o/r_1)^2 B_{ro} + \Delta B_{r1}$. Substituting into (8), using equation (5) and rearranging gives the kinematic contribution to excess flux:

$$\Delta F_S(r) = 2\pi r_1^2 \Delta B_{r1}\left[\frac{\mu(r - r_o) - 1}{\mu_1(r_1 - r_o)}\right] \quad (9)$$

All of the above equations assume that solar wind speed V does not depend on r but, as discussed above, when $dV > 0$ dynamical effects become important. This applies to the corotating interaction regions, as well as to temporal cases such as ahead of coronal mass ejections (CMEs). These dynamical effects are absent in rarefaction regions ($dV < 0$) because the faster flow runs ahead of the slow flow. Hence it is instructive to repeat the distribution shown in gray in Figure 2 for values of $c\Delta B_r$, for which c removes the effect of the polarity of $B_{\varphi r}$: hence $c\Delta B_r > 0$ corresponds to $dV > 0$ (compression regions) and $c\Delta B_r < 0$ corresponds to $dV < 0$ (rarefaction regions). This is shown by the black line in Figure 2. It can be seen that the symmetric distribution for $c = +1$ has become slightly asymmetric with slightly lower numbers of samples giving large positive $c\Delta B_r$ than give large negative $c\Delta B_r$ of the same magnitude. This is consistent with the asymmetry expected for the dynamical stream–stream interaction effects which will be present in compression regions only. Thus we can conclude that using 1-day means to derive (dV/dt) has removed much, but not all, dynamical effects in the excess flux calculation. Because measurement uncertainties and our assumptions can sometimes (in <1% of hourly means) cause exceptionally large values of $|\Delta B_r|$, we here exclude from the survey all samples which are more than 3σ from the mean (the standard deviation from Figure 2 being σ = 2.24 nT).

[13] Taking the integral of all the 87,759 available hourly positive $c\Delta B_r$ values in Figure 2 up to this 3σ limit (i.e., in the compression regions) we get 0.33 Ts, whereas the corresponding integral value for all the 99,694 hourly negative $c\Delta B_r$ values (i.e., in the rarefaction regions where $dV < 0$) is −0.40 Ts. Because there are no stream–stream interaction effects in the rarefaction regions, and because the true integrated excess flux effect for $dV > 0$ regions should be equal and opposite to that for $dV < 0$: we can infer that the dynamical interactions have caused the procedure described above to underestimate the kinematic effect in compression regions by a factor 100(0.40–0.33)/0.40% = 17.5%, on average. Given the $dV > 0$ regions are present for 46.8% of the time, we can estimate that we may have underestimated the kinematic excess flux effect by some 0.468 × 17.5 = 8.2%, on average. In theory, we could use Figure 2 to calibrate for this effect and remove the average residual dynamic interaction effects in compression regions: however, we do not attempt to implement such an average correction here and instead note the average level of

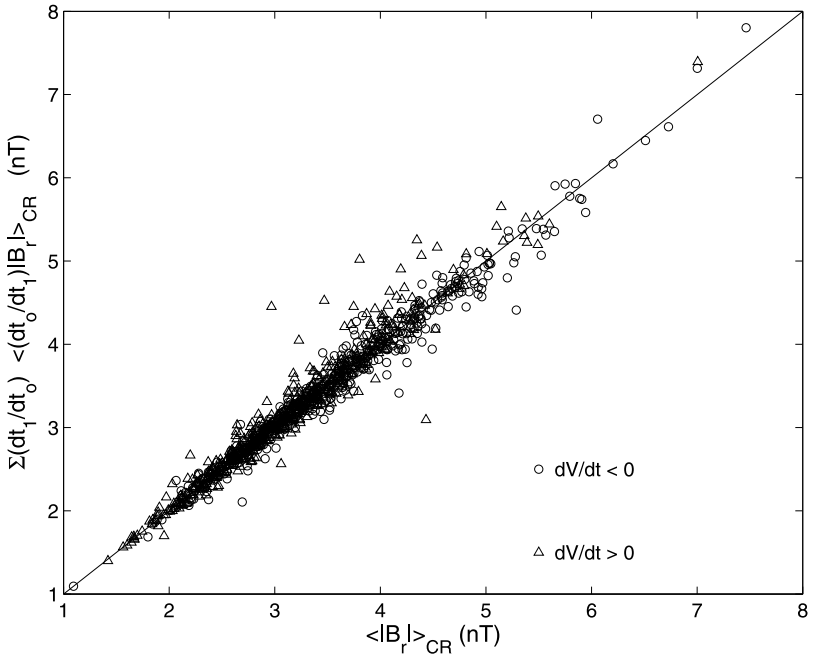

Figure 5. Analysis of the effect of kinematic bunching on the sampling of radial field values. Averages for Bartels rotations are shown for the entire Omni-2 data set for 1963–2008. The abscissa shows the mean radial field seen by near-Earth spacecraft ($r = r_1 = 1$ AU) for sampling intervals $dt_1 = 1$ h, $\langle|B_r|\rangle$. The ordinate gives the mean for the weighted observed radial field values, for a weighting factor of (dt_o/dt_1), where dt_o is the time separation at $r = r_o$ which corresponds to dt_1. Triangles are for data in compression regions, $dV/dt > 0$, giving $dt_o > dt_1$; circles are for data in rarefaction regions, $dV/dt > 0$, for which $dt_o < dt_1$. The raw data means and the weighted means are equal along the diagonal line. It can be seen that the sampling bias introduced by compression/rarefaction during one solar rotation is generally (but not always) very small and that no bias is introduced on average. Almost no difference is seen in average values between compression and rarefaction regions.

underestimation of the kinematic effect owing to dynamical effects in compression regions.

3. Kinematic Effects on Sampling

[14] The kinematic effects discussed in section 2 cause a bias in the sampling of the IMF/slow wind seen in the heliosphere [*McComas et al.*, 1992]. Regions of $[\partial V/\partial t]_o > 0$ give $dt < dt_o$, which means that a satellite at $r > r_o$ will sample the resulting compression regions relatively more often than at the source region. Conversely regions of $[\partial V/\partial t]_o < 0$ give $dt > dt_o$ and so fewer of the regular samples at the satellite will relate to these rarefaction regions, compared to at the source region. Hence if the field at the source surface is systematically different in the regions of $[\partial V/\partial t]_o > 0$, this would introduce a bias into the averages seen at $r > r_o$.

[15] From equation (6) the value of dt_o corresponding to the sampling interval dt_1 can be calculated for all the Omni-2 data from $r = r_1$, with the kinematic assumption that V is independent of r. In addition to the conventional mean for a solar rotation, $\langle|B_{r1}|\rangle_{CR}$, we can compute a mean where each sample of $|B_{r1}|$ is weighted by a factor $w = (dt_o/dt_1)/\{\Sigma_{CR}(dt_o/dt_1)\}$, which means it is weighted by the time interval relevant to at the source surface, rather than that at the point of observation. Figure 5 is a scatterplot of $\langle|B_{r1}|\rangle_{CR}$ and $\langle w\,|B_{r1}|\rangle_{CR}$ which shows there is no systematic difference between the two. Circles are averages for data in rarefaction regions ($dV < 0$) whereas the triangles are for compression regions ($dV > 0$). Individual solar rotations may show some deviation of $\langle w|B_{r1}|\rangle_{CR}$ from $\langle|B_{r1}|\rangle_{CR}$, and there is a slight tendency for the biggest deviations to be in compression regions. The scatter for this plot (which considers the difference between $r_o = (2.5/251)$AU and $r_1 = 1$ AU) is somewhat greater than for the corresponding plot (Figure 5) in paper 1 for between $r_1 = 1$ AU and Ulysses at $r_U \approx 1.5$ AU. We believe that this is partly because the range of r is greater and includes the solar wind acceleration region. However, on average, $\langle w|B_{r1}|\rangle_{CR}$ and $\langle|B_{r1}|\rangle_{CR}$ still agree very closely for both $dV > 0$ and $dV < 0$. As in paper 1, we can conclude that kinematic effects have not introduced a bias and this conclusion is not effected by dynamical effects in interaction regions (which are absent in rarefaction regions). Hence we can eliminate the kinematic bunching effect on sampling as a contributor to the flux excess. We have confirmed this conclusion using the theoretical model of kinematic structures developed by A. P. Rouillard and M. Lockwood (Solar stream magnetism: Analytic prediction of three-dimensional heliospheric fields and flows, submitted to *Astronomy and Astrophysics*, 2009).

4. Kinematic Effect on the Radial Field and Flux Excess

[16] Figure 2 shows the distribution of hourly ΔB_r values computed using equation (6) for all the near-Earth ($r \approx r_1 =$ 1 AU) observations between 1963 and 2008 in the Omni-2

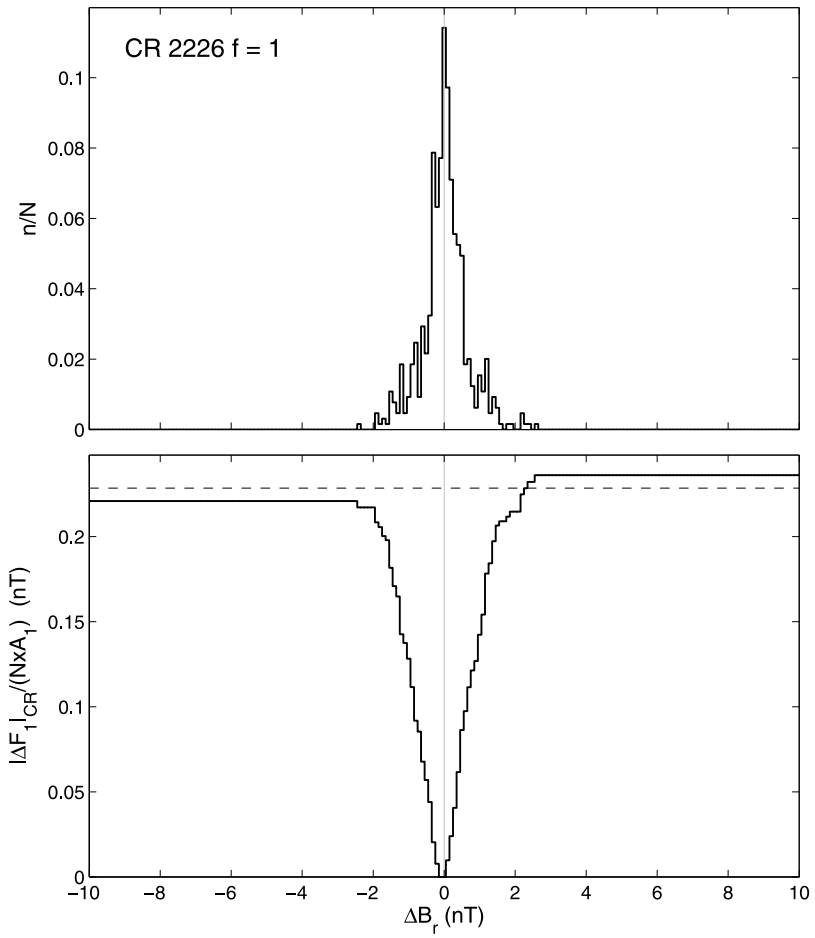

Figure 6. (top) The same as Figure 2 but for a single Bartels rotation (in this example, number 2226). The number of hourly Omni-2 data points giving a predicted additional radial field of $[\Delta B_{r1}]_k$ is n_k. The fraction of the total possible number ($N = 27 \times 24$) of hourly samples available for this particular solar rotation is $f = \Sigma_k(n_k/N) = 1.0$; that is, there are no data gaps in this case. (bottom) The ordinate is $[\Delta F_1]_{CR}/(NA_1)$, where $[\Delta F_1]_{CR}$ is the magnitude of the integrated additional radial field up to the limit $[\Delta B_r]_i$ (abscissa); i.e., $[\Delta F_1]_{CR} = \Sigma^i_{kk=0} A_1 n_k|\Delta B_{r1}|_k$, where A_1 is the area of the surface of the heliocentric sphere of radius r_1 that is swept out by unit length in the N direction (of the RTN coordinate system) by solar rotation during 1 h. The value at $[\Delta B_{r1}]_i = -10$ nT is the predicted total of all detected inward extra flux $[\Delta F_1]_{in}$ and that at $[\Delta B_{r1}]_i = +10$ nT is the corresponding integrated outward flux $[\Delta F_1]_{out}$. For stationary conditions over the solar rotation, with purely radial flow and no vestigial net effect of stream–stream interactions, we would expect $[\Delta F_1]_{in} = [\Delta F_1]_{out}$ and the mean additional radial field produced by kinematic effects would be $|\Delta B_{r1}|_{CR} = 2[\Delta F_1]_{in}/(NA_1) = 2[\Delta F_1]_{out}/(NA_1)$. The dashed horizontal line shows the average of $[\Delta F_1]_{in}$ and $[\Delta F_1]_{out}$ which is here taken to be $(NA_1)\ |\Delta B_{r1}|_{CR}/2$.

data set. In order to evaluate the net effect over each solar rotation, we plot the equivalent distributions, an example being given in Figure 6 (top). As discussed in paper 1, it is valuable to use integer 27-day intervals and so we use Bartels rotation intervals rather than Carrington rotations (the former being 27 days the latter 27.2753 days). This particular example is for Bartels rotation number 2226. The number of hourly Omni-2 data points giving a predicted additional radial field of $[\Delta B_r]_k$ is termed n_k and so the fraction of the total possible number ($N = 27 \times 24$) of hourly samples available for this particular solar rotation is $f = \Sigma_k n_k/N = 1.0$; that is, there are no data gaps in this case. It can be seen that the distribution is quite symmetric (i.e., roughly half the predicted extra flux generated by kinematic effects is outward and half is inward), but the distribution is not as symmetric as the equivalent plot in Figure 2 (the gray area for $c = +1$) which is for all the data.

[17] To evaluate the effect of this extra inward/outward flux on the $\langle|B_{r1}|\rangle_{CR}$ and open flux estimates, we here compute the integral from zero to each additional radial field of $[\Delta B_r]_i$, giving a magnetic flux of $[\Delta F_1]_{CR} = \Sigma^i_{kk=0} A_1 n_k|\Delta B_r|_k$ (where A_1 is the area of the surface of the heliocentric sphere of radius r_1, that is swept out by unit latitudinal length by solar rotation during the hour). Figure 6 (bottom) shows $[\Delta F_1]_{CR}/(NA_1)$ as a function of $[\Delta B_r]_i$. The value at $[\Delta B_r]_i = -10$ nT is the total

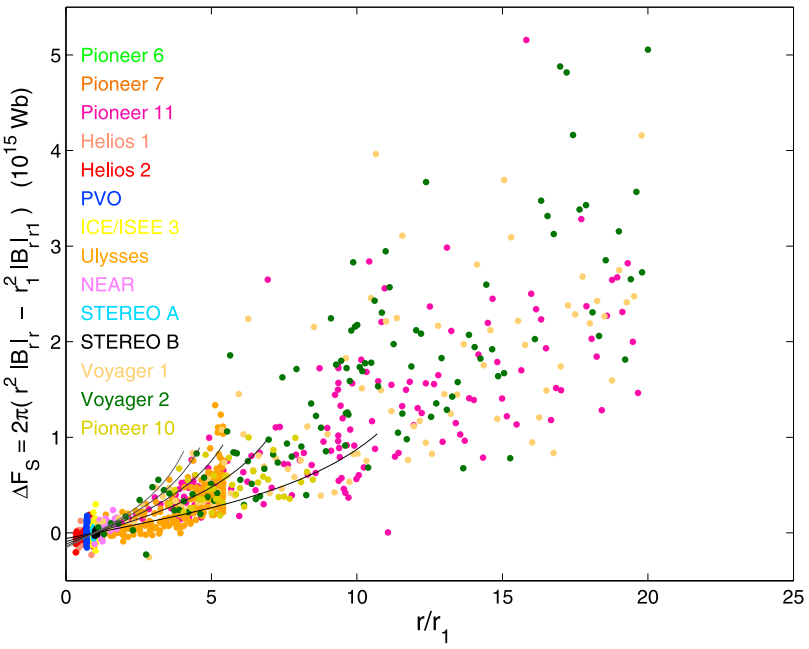

Figure 7. The observed additional open flux ΔF_S as a function of r/r_1. The colored dots are the differences between full solar rotation averages observations from various spacecraft, compared with the coincident Omni-2 data value. The lines are from the predicted $|\Delta B_{r1}|_{CR}$ from the Omni-2 data using the mode value of the distribution shown in Figure 3 (see text). The lines show the ΔF_S values which would be exceeded a fraction p of the time where p is 0.1 (for black line), 0.25, 0.5, 0.75 and 0.9 (light gray line).

of all predicted inward extra flux $[\Delta F_1]_{in}$ during the solar rotation in question and that at $[\Delta B_r]_i$ = +10 nT is the corresponding integrated outward extra flux $[\Delta F_1]_{out}$. In this case $[\Delta F_1]_{in}$ is slightly smaller than $[\Delta F_1]_{out}$: for some other solar rotations it is the other way round and only relatively rarely are the two exactly equal. For stationary conditions over the solar rotation, with purely radial flow and no residual contributions of dynamic effects in compression regions, we would expect $[\Delta F_1]_{in} = [\Delta F_1]_{out}$ and the mean additional radial field produced by kinematic effects would then be $|\Delta B_r|_{CR} = 2[\Delta F_1]_{in}/(NA_1) = 2[\Delta F_1]_{out}/(NA_1)$, the factor of 2 arising because both the inward and outward flux contribute to the absolute value of the radial field. We attribute the differences between $[\Delta F_1]_{in}$ and $[\Delta F_1]_{out}$ detected to either nonstationary conditions over the solar rotation, to residual dynamical effects, to data gaps and/or to nonradial flow. We here take the arithmetic mean of $[\Delta F_1]_{in}$ and $[\Delta F_1]_{out}$ (the dashed horizontal line in Figure 6 (bottom)) to be equal to $(NA_1)\ |\Delta B_{r1}|_{CR}/2$. Using this estimate of $|\Delta B_{r1}|_{CR}$ will introduce some scatter into the values for individual solar rotations, but which should average out when sufficient solar rotations are considered together (e.g., in annual means).

[18] Figure 7 shows solar rotation averages of the observed flux excess ΔF_S, computed as a function of r using equation (8), from a survey of data from a number of spacecraft throughout the heliosphere. This is an updated version of *Owens et al.* [2008a, Figure 1]. Points are colored according to the spacecraft giving the observations away from 1 AU, as given by the key. The simultaneous data from 1 AU is taken from the Omni-2 data set. It can be seen the excess flux increases with r as does the scatter about the trend.

[19] The lines in Figure 7 are predicted using the theory given in section 2 in the following manner. The values of $|\Delta B_{r1}|_{CR}$ for each solar rotation are computed (as demonstrated by Figure 6) and from the distribution of these solar rotation values are taken the upper and lower deciles, the upper and lower quartiles and the median (i.e., the probability of $|\Delta B_{r1}|_{CR}$ exceeding these values is p equal to 0.9, 0.1, 0.75, 0.25 and 0.5). These five values are then used to generate the corresponding $|\partial V/\partial t|_o/V^2$ values using the mode value of the distribution shown in Figure 4 (which is m = 0.2 AU^{-1} nT^{-1}). These are then used to generate a pair of $\mu(r)$ profiles for each of the 5 p values using equation (7) with $[\partial V/\partial t]_o/V^2 = \pm\ m\ |\Delta B_{r1}|_{CR}$ (the plus being for compression regions, the minus being for rarefaction regions). These are then averaged together and the average $\mu(r)$ profile is then used with equation (9) to extrapolate each of the above five values to other r. Extrapolation has been curtailed at the point where the compression regions are tending toward giving infinite field as this is where the kinematic disturbance would steepen into a shock [*Burlaga et al.*, 1983].

[20] Thus we can predict the flux excess ΔF_S that we would expect at a given r to be exceeded with a probability p of 0.1, 0.25, 0.5, 0.75 and 0.9 of the time. These are the five lines in Figure 7 (shaded from black to light gray). It can be seen that these fit the observations reasonably well and shows that the flux excess is indeed consistent with the kinematic effects described in section 2. The spread of the

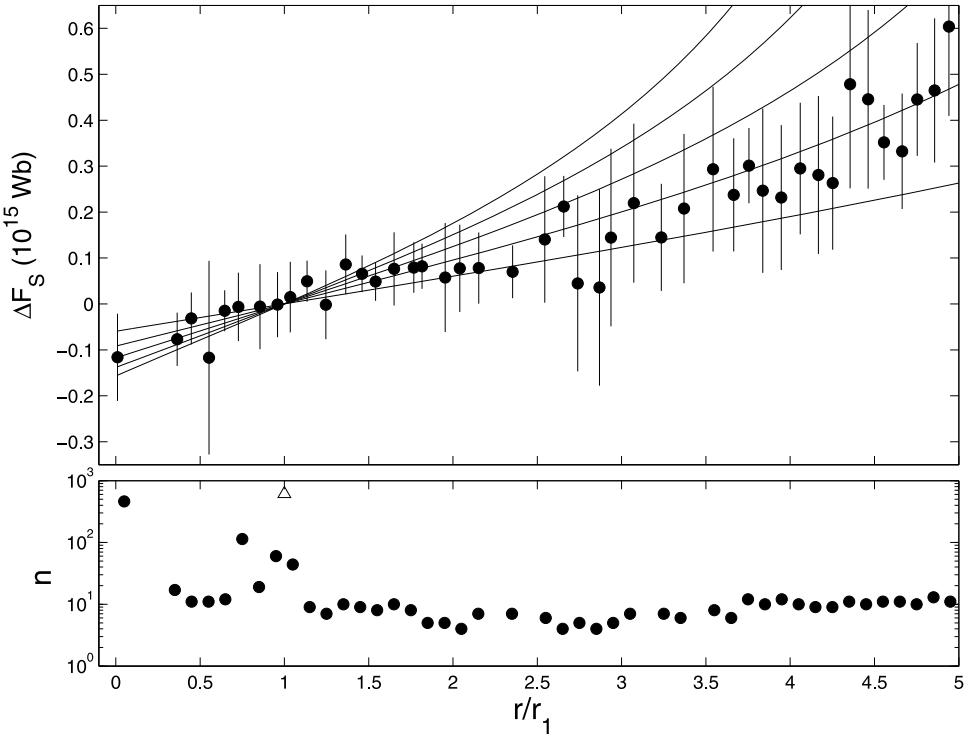

Figure 8. (top) The additional open flux ΔF_S as a function of r/r_1, where r is the heliocentric distance and r_1 = 1 AU. The data points show the mean values from the spacecraft data shown in Figure 7, averaged over r bins 0.1 AU wide, with error bars of plus and minus one standard deviation. The lines are the same as shown in Figure 7. The data point at the lowest r/r_1 is the entire PFSS data set for the coronal source surface at $r = r_o$. (bottom) The number of full solar rotation averages n contributing to the means. The open triangle shows the number in the Omni-2 data set from $r = r_1$. Note that n is shown on a logarithmic scale.

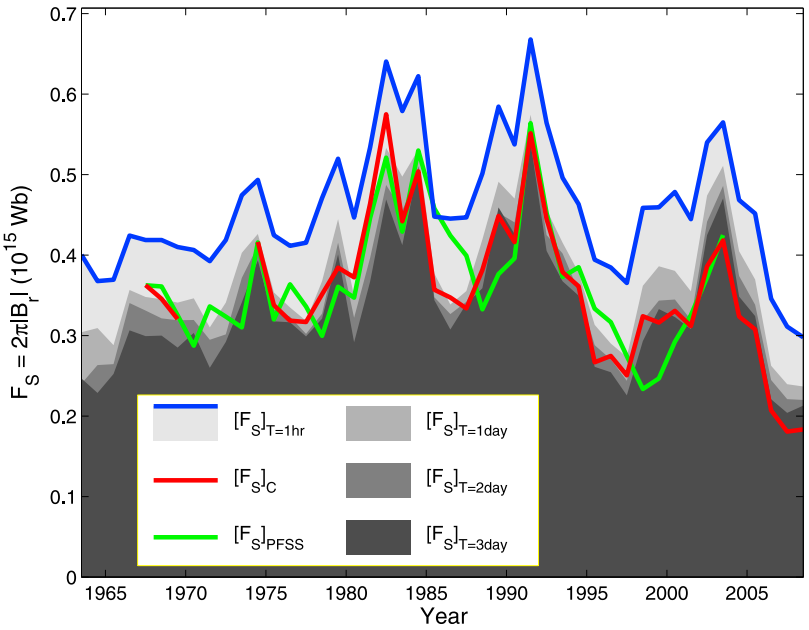

Figure 9. The gray shaded areas show annual means of the signed open solar flux from the Omni-2 data $[F_S]_T = 2\pi\, r_1^2\, \langle |B_{r1}|_T \rangle$, with absolute values taken of means on timescale T. The light gray area bounded by the blue line is for T = 1 h ($[F_S]_{T\,=\,1hr}$) and successively darker gray areas are for T = 1, 2, and 3 days. The green line is the corresponding value from the PFSS data, mapped to $r = r_1$, with no allowance for kinematic effects, $[F_S]_{PFSS}$. The red line shows the Omni-2 values for T = 1 h, minus the correction term for kinematic effects, $[F_S]_C = 2\pi r_1^2\, \{\langle |B_r|_{T\,=\,1hr} \rangle_{CR} - \langle \Delta B_{r1} \rangle_{CR}\}$.

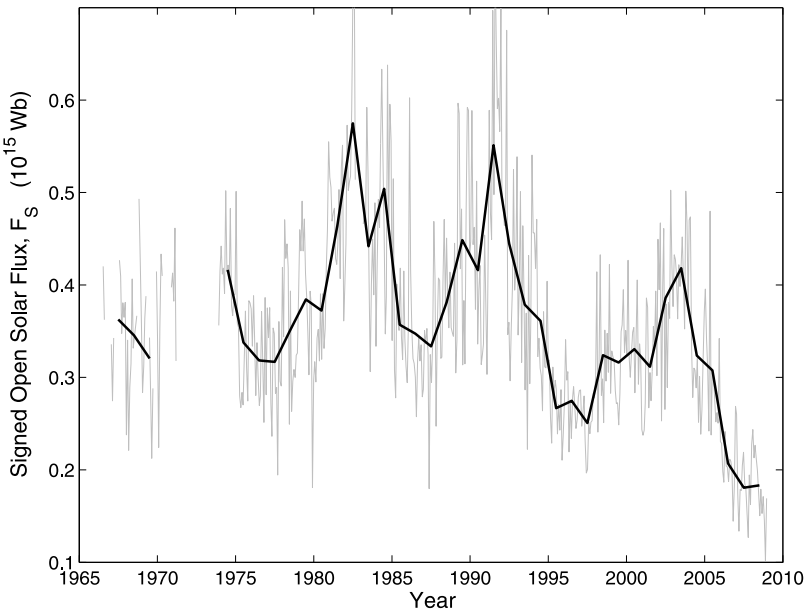

Figure 10. The signed open solar flux, corrected for the excess flux using the kinematic effect discussed in this paper, $[F_S]_C = \langle [F_S]_{T\,=\,1hr} \rangle_{CR} - 2\pi\, r_1^2 |\Delta B_r|_{CR}$. Annual means are shown by the thick black line (also shown by the red line in Figure 9); averages over Bartels rotations are shown by the thin gray line.

lines for different p matches the observed scatter reasonably well.

[21] Figure 8 shows the data from Figure 7 for $r < 5$ AU. Instead of individual solar rotation values of ΔF_S, means for bins of r that are 0.1 AU wide are shown with error bars of plus and minus one standard deviation. Figure 8 (bottom) shows the number of solar rotation averages in each bin (on a logarithmic scale). The five lines are the same as in Figure 7. By definition of ΔF_S, all five lines pass through zero at $r = 1$ AU. In addition to the satellite data from Figure 7, the mean and standard deviation of all PFSS values are shown by the leftmost data point in Figure 8. It can be seen that the flux excesses for these PFSS estimates lie on the same trend with r as do the satellite data (and are negative; i.e., the PFSS values are lower than those from $r =$ 1 AU). We therefore infer that the tendency for lower PFSS values noted by *Wang and Sheeley* [1995] and *Lockwood et al.* [2006] has the same origin as those noted in spacecraft data by *Owens et al.* [2008a] and both are consistent with kinematic effects introduced by large-scale spatial velocity gradients.

5. Long-Term Variations in Open Solar Flux

[22] Figure 9 shows annual means of the open flux derived for averaging timescales T of 1 h, 1 day, 2 days and 3 days (gray shaded areas). The red line shows the variation for $T = 1$ h, minus the kinematic correction $|\Delta B_{r1}|_{CR}$ derived as described above, $[F_S]_C = 2\pi r_1^2 \{\langle [B_r]_{T\,=\,1hr} \rangle_{CR} - \langle \Delta B_{r1} \rangle_{CR}\}$. Note that because this correction uses the observed tangential field value $B_{\varphi r1}$ at $r = r_1$ with equation (5), it does not rely on the average procedure used to obtain $\mu(r)$ and hence generate the $\Delta F_S(r)$ profiles in Figures 7 and 8. The green line shows the values derived from magnetograph data using the PFSS method [*Wang and Sheeley*, 1995], $[F_S]_{PFSS}$. Additional data gaps appear early in the corrected data sequence (in red) because we require both IMF and solar wind data and we set a requirement 50% data availability. It can be seen that the corrected open flux values match the PFSS data rather well, better than those obtained using T of 1–3 days. The r.m.s. difference between the PFSS values and the kinematically corrected open flux values is 4.1×10^{13} Wb, whereas the corresponding r.m.s. difference for using averaging over $T = 1$ day is 6.9×10^{13} Wb. Thus the kinematic correction performs better on average but not dramatically so.

[23] Last, Figure 10 shows the variation of solar rotation averages (thin dark gray line) and annual means (thick black line) of the open solar flux, corrected for the kinematic effects, as described above. The most notable feature is how rapid the descent of open solar flux has been over recent cycles. The annual mean open flux for 1987 is a solar minimum value of 0.382×10^{15} Wb, whereas the annual mean open flux in 2007, also a solar minimum value, is 0.198×10^{15} Wb. In other words, the annual mean open solar flux was 93% higher in 1987 than it was in 2007.

6. Discussion and Conclusions

[24] The analysis presented here has shown that the flux excess seen by various spacecraft in the inner heliosphere (mainly close to the ecliptic plane) is consistent with the difference between values derived using in situ data from heliocentric distances of $r \approx 1$ AU compared to those deduced from solar magnetograph data using the PFSS method. In addition, we have shown both are consistent with kinematic effects in the streamer belt owing to large-scale (timescales $T > 1$ day) longitudinal structure in the solar wind flow.

[25] There is no kinematic effect unless there is a tangential seed field in the region of high solar wind speed shear. The origin of such tangential seed fields could be, for example, near-Sun interchange reconnection of magnetic field or could be faster flow emerging beneath overdraped Parker spiral field (temporal effects such as CMEs). Because the analysis starts from the observed field at r near 1 AU and maps back to the source surface ($r = r_o$), our results do not depend on the mechanism which generates the tangential seed field in the first instance. We have investigated the effect of the biggest assumption made (that V does not depend on r; i.e., assuming that dynamical stream–stream interaction effects have been largely removed by the 1-day smoothing time constant applied to the observed velocity gradient) and found that the resulting difference between compression and rarefaction regions is small. We conclude the vestigial effects of stream–stream interactions in our kinematic correction terms are small and tend to cancel out.

[26] Figure 9 shows that the temporal variation of the annual mean of the corrected open flux $[F_S]_C$, derived by applying the kinematic correction for excess flux to whole-solar rotation data from spacecraft near 1 AU, matches very well that from PFSS modeling on the basis of magnetograph data. In particular, the two agree somewhat better than applying by preaveraging over a fixed interval T. Up until about 1986 (solar cycles 20 and 21), using T = 1 day ($[F_S]_{T = 1\ day}$) matches the PFSS data rather well; however, over cycle 22 $[F_S]_{T = 2\ day}$ matches better and over cycle 23 even $[F_S]_{T = 3\ day}$ does not give an adequate correction. As discussed in the introduction, there will, at any one time, be a T value for which the derived open flux at 1 AU equals the correct value at the source surface; however, Figure 9 implies that the optimum T at 1 AU has changed. The agreement with PFSS open flux estimates is improved somewhat if we use the kinematic correction rather than averaging over intervals of T = 1 day (the r.m.s. deviation is reduced by about a third).

[27] Paper 1 showed that small-scale structure (timescales less than 1 h) does not contribute to flux excess, but structure on timescales between 1 h and 1 day could still be a factor: the use of means over, for example, T = 1 day would be the best way to remove such structure. Because of dynamical interactions, our analysis of kinematic effects needs to smooth the observed velocity gradients (we use a time constant of 1 day) and so we here have predicted the kinematic effects of flow structure on timescales of >1 day. These can match the observed flux excess, and its variations with r and time, rather well. However, we cannot eliminate the possibility that there is a contribution to the excess flux from structure on timescales between 1 h and 1 day (at least some of which could come from dynamical effects). In this discussion about the physical origin of the flux excess, it is interesting to note the latitudinal difference reported in paper 1: that the flux excess was considerably greater in the streamer belt than outside it. *Lockwood and Owens* [2009] show that, in fact, this only applies around sunspot minimum and that near sunspot maximum the flux excess is roughly as great at high heliographic latitudes as at low latitudes. This clearly points to kinematic and/or dynamical interaction effects as the physical origin of the flux excess. Naturally, in general, one cannot have one without the other. However, here we have used smoothing to damp the dynamical effects (and shown that this is approximately achieved because rarefaction and compression show similar results) and find a close agreement of the data with the kinematic effects predicted for the background the solar wind flow structure on timescales of >1 day. However, this does not eliminate contributions to the excess flux of structure in the field from another source on timescales in the range 1 h to 1 day.

[28] Figure 9 shows that the open solar flux in the current solar minimum is lower than at any previous time since measurements of interplanetary space began in 1963, and that rapid descent has occurred since the maximum of the long-term variation in open solar flux in 1987 identified by *Lockwood* [2001, 2003] and *Lockwood and Fröhlich* [2007]. Here we note, the correction $2\pi r_1^2|\Delta B_{r1}|_{CR}$ (needed to match PFSS values) has increased slightly in magnitude. Note that the low values of open fluxes for the current solar minimum do not only originate from data from the ACE and WIND spacecraft (which are the major contributors to the Omni-2 data at this time): Paper 1 shows that they are consistent with the Ulysses data at larger r and *Owens et al.* [2008a] have shown that values from the two STEREO craft, at similar r but different solar longitude φ, are almost identical.

[29] A number of models for the evolution of the heliospheric magnetic field have been proposed. *Fisk et al.* [1999] argue that the Sun's open flux tends to be conserved, with "interchange reconnection" [see *Crooker et al.*, 2002] between open and closed solar fields resulting in an effective diffusion of open flux across the solar surface without, necessarily, any net change in the total open flux. In this case, the heliospheric field evolves with simple rotation of regions of positive and negative polarity separated by a single, large-scale heliospheric current sheet [*Fisk and Schwadron*, 2001; *Jones et al.*, 2003]. Alternatively, it has been argued that emerging midlatitude bipoles cause closed coronal loops to rise and first destroy preexisting open flux in the polar coronal hole (remnant from the previous solar cycle) and then build up a new polar coronal hole (of the opposite polarity) and so reverse the polar field of the Sun [*Babcock*, 1961; *Wang and Sheeley*, 2003], which fits well with the migration of photospheric fields inferred from magnetograph data. The evolution of the heliospheric magnetic field could also be facilitated by transient events [*Low*, 2001]: specifically, *Owens et al.* [2007] and *Owens and Crooker* [2006, 2007] investigate the role of the magnetic flux contained in coronal mass ejections (CMEs) in the observed variation in flux seen by craft in the heliosphere. These different concepts are not mutually exclusive in many respects (see review by *Lockwood* [2004]).

[30] Much of the difference between these concepts is a matter of semantics. "Open flux" has here, and in many previous papers, been taken to be the same as "coronal source flux;" that is, the magnetic flux that leaves the solar atmosphere and enters the heliosphere by threading the coronal source surface at 2.5 solar radii. It is a readily measurable quantity because of PFSS modeling (within the assumptions of that technique) and because the Ulysses result allows the use of in situ magnetic field data (but we have shown that some form of correction is needed for the

excess flux effect). This is quite different from another definition of open flux which requires that it has only one foot point still attached to the Sun [e.g., *Schwadron et al.*, 2008]. Flux which appears to be in this category can sometimes be inferred for in situ point measurements, for example from heat flux or unidirectional "strahl" electron distribution functions, although scattering by heliospheric structure into other populations such as "halo" often makes this far from unambiguous [*Larson et al.*, 1997; *Fitzenreiter et al.*, 1998; *Owens et al.*, 2008c]. Even if this could be done reliably, there is no way to quantify the total of such flux at any one time from such in situ point measurements. This is because there is no equivalent of the Ulysses result (and so no equivalent to equation (1) for this flux) to generalize in situ point measurements into a global quantity. To make the distinction clear, let us here refer to these two definitions as the "total open flux" F_S (defined by equation (1)) and the "single–foot point open flux" F_O. The latter is a subset of the former. The only topological distinction that F_O can have which separates it from other heliospheric flux (the $F_S - F_O$ of double–foot point open flux) is that it threads the heliopause and enters interstellar space. (Note that any other definition involving any boundary within the heliosphere will cause the continuous conversion of the flux ($F_S - F_O$) into F_O as the magnetic flux frozen-in to the solar wind flow propagates through that boundary).

[31] Until we can quantify F_O, there can be no evidence that it is constant and thus the idea that it is constant can be no more than a hypothesis. Confusingly, it has been claimed that the total open flux F_S is constant and that this is evidence that the single–foot point open flux F_O is constant. The key point we wish to underline here is that F_S is far from constant.

[32] Coronal mass ejections are an important example (but not the only example) of flux that undoubtedly contributes to F_S but may not contribute to F_O [*Mackay and van Ballegooijen*, 2006]. Consider a magnetic flux tube which is an element of a CME and which contains a magnetic flux F_E. It will enhance the flux F_S by $2F_E$ (F_E at each foot point), once it has propagated beyond the coronal source surface without any foot point disconnection. This emergence does not change F_O. However, unless F_S is to increase indefinitely with continuing CME emergence, other processes must occur. Emergence followed by subsequent reconnection with a preexisting similar loop (i.e., with dual–foot point open flux which is part of F_S but not part of F_O) will give no net change in either F_S or F_O. Emergence with subsequent disconnection in one hemisphere A by magnetic reconnection with preexisting single–foot point open field (residual from the previous solar cycle and thus with the opposite polarity) will also give no net change in neither F_S nor F_O. (Note that single–foot point flux of the old polarity attached to hemisphere A has decreased by F_E whereas the new polarity flux attached to hemisphere B has increased by the same amount; i.e., this is foot point exchange). If reconnection of CME flux with single–foot point open flux can occur in hemisphere A, there is no reason why sometimes it cannot also occur in the other hemisphere B (either simultaneously or, more likely, sometime before/after). Emergence followed by complete foot point disconnection (in both hemispheres) causes both F_S and F_O to fall by $2F_E$. The CME processes therefore acts to either conserve or decrease F_O. If F_O is decreased, the counterbalancing source would be reconnection at the heliopause of dual–foot point open flux ($F_S - F_O$) with the magnetic field in interstellar space (which increases F_O but does not alter F_S). This would be, at most, only distantly related to the near-Sun processes.

[33] The time series of the total open flux F_S shown in this paper (Figure 10) and by prior publications reveals that there is considerable variation. The total open solar flux at solar minimum fell from an annual mean of 3.82×10^{16} Wb in 1987 to close to half that value (1.98×10^{16} Wb) in 2008.

[34] Long-term variations in the total open solar flux F_S have previously been inferred from historic geomagnetic data by *Lockwood et al.* [1999a, 1999b], *Lockwood* [2001, 2003] and *Rouillard et al.* [2007], showing that the open solar flux roughly doubled between 1900 and about 1950. It has been claimed that this rise was an artifact of the *aa* geomagnetic data [*Svalgaard et al.*, 2003, 2004] or was present but much smaller in magnitude [*Svalgaard and Cliver*, 2007]. Analysis using a wide variety geomagnetic data show neither to be the case [e.g., *Rouillard et al.*, 2007]. In this debate, the important difference between open solar flux F_S (and hence by equation 1 the radial field component) and the heliospheric field strength B has also often been overlooked. As a result, discussion of the existence [*Svalgaard and Cliver*, 2005], or otherwise [*Owens et al.*, 2008b], of a "floor" minimum to B is irrelevant. *Rouillard et al.* [2007] pointed out the role of even uniform solar wind flow speed V in decoupling F_S and B. (In Parker spiral theory, increased/decreased V causes the spiral to unwind/wind up and so B falls/rises for a fixed F_S). But these authors point out this is not the only effect which in the past has been accounted for using the timescale T [*Rouillard et al.*, 2007; *Lockwood et al.*, 2006]. In the present paper, we have shown that this additional effect is consistent with longitudinal structure in the solar wind flow which gives the kinematic flux excess effect.

[35] The long-term change in the open flux deduced from geomagnetic activity has been reproduced by a number of numerical models of flux continuity and transport during the solar magnetic cycle, given the variation in photospheric emergence rate indicated by sunspot numbers [*Solanki et al.*, 2000, 2002; *Schrijver et al.*, 2002; *Lean et al.*, 2002; *Wang and Sheeley*, 2003; *Wang et al.*, 2005]. The principle laid down by *Solanki et al.* [2000, 2002] is that total open flux F_S obeys a continuity equation, with the rate of change being the difference between a source terms (the total rate that coronal field loops emerge through the coronal source surface, including CMEs) and loss terms owing to field reconfiguration and disconnection by magnetic reconnection. The discussion above about CME effects illustrates that several different topologies of disconnection must be active (see review by *Lockwood* [2004]). In the absence of known mechanisms that could make the total loss (from the variety of mechanisms) exactly equal to the simultaneous production rate, we must expect the total open flux to vary on a variety of timescales.

[36] In this context, it is worth noting that the annual mean solar minimum open solar flux, derived here with correction for kinematic effects, was almost twice as large in 1987 than it was in 2007. This means that the observed fall

in the minimum value over the last two solar cycles was considerably faster than the rise inferred from geomagnetic activity observations over four solar cycles in the first half of the 20th century.

[37] **Acknowledgments.** All three authors are supported by the UK Science and Technology Facilities Council. We are also grateful to the Space Physics Data Facility and the National Space Science Data Center for provision of the Omni-2 data set and to many scientists who contributed to both Omni-2 and to other magnetic field observations used here: from Pioneer 6 and 7 (principal investigator N. Ness), Pioneer 10 and 11 (principal investigator E. Smith), Pioneer Venus Orbiter (principal investigator C. Russell), Helios (principal investigator N. Ness), Voyager (principal investigator L. Burlaga), ICE-ISEE3 (principal investigator E. Smith), Ulysses (principal investigator A. Balogh), and STEREO (principal investigator M. Acuña), and to the Small Bodies Node of the Planetary Data System for NEAR magnetometer data (principal investigator M. Acuña). We also thank Yi-Ming Wang for the provision of the PFSS data.

[38] Amitava Bhattacharjee thanks the reviewers for their assistance in evaluating this paper.

References

Altschuler, M. A., and G. Newkirk Jr. (1969), Magnetic fields and the structure of the solar corona, *Sol. Phys.*, *9*, 131–149, doi:10.1007/BF00145734.

Arge, C. N., and V. J. Pizzo (2000), Improvement in the prediction of solar wind conditions using near-real time solar magnetic field updates, *J. Geophys. Res.*, *105*, 10,465–10,479, doi:10.1029/1999JA000262.

Babcock, H. W. (1961), The topology of the Sun's magnetic field and the 22-year cycle, *Astrophys. J.*, *133*, 572–587, doi:10.1086/147060.

Burlaga, L. F., and E. Barouch (1976), Interplanetary stream magnetism: Kinematic effects, *Astrophys. J.*, *203*, 257–267, doi:10.1086/154074.

Burlaga, L. F., R. Schwenn, and H. Rosenbauer (1983), Dynamical evolution of interplanetary magnetic fields and flows between 0.3 and 8.5 AU—Entrainment, *Geophys. Res. Lett.*, *10*, 413–416, doi:10.1029/GL010i005p00413.

Couzens, D. A., and J. H. King (1986), Interplanetary medium data book, *Suppl. 3*, Natl. Space Sci. Data Cent., Goddard Space Flight Cent., Greenbelt, Md.

Cranmer, S. R. (2002), Coronal holes and the high-speed solar wind, *Space Sci. Rev.*, *101*, 229–294, doi:10.1023/A:1020840004535.

Crooker, N. U., J. T. Gosling, and S. W. Kahler (2002), Reducing heliospheric magnetic flux from coronal mass ejections without disconnection, *J. Geophys. Res.*, *107*(A2), 1028, doi:10.1029/2001JA000236.

Fisk, L. A., and N. A. Schwadron (2001), The behaviour of the open magnetic field of the Sun, *Astrophys. J.*, *560*, 425–438, doi:10.1086/322503.

Fisk, L. A., T. H. Zurbuchen, and N. A. Schwadron (1999), Coronal hole boundaries and their interaction with adjacent regions, *Space Sci. Rev.*, *87*, 43–54, doi:10.1023/A:1005153730158.

Fitzenreiter, R. J., K. W. Ogilvie, D. J. Chornay, and J. Keller (1998), Observations of electron velocity distribution functions in the solar wind by the Wind Spacecraft: High angular resolution Strahl measurements, *Geophys. Res. Lett.*, *25*, 249–252, doi:10.1029/97GL03703.

Gosling, J. T. (1996), Co-rotating and transient solar wind flows in three dimensions, *Annu. Rev. Astron. Astrophys.*, *34*, 35–73, doi:10.1146/annurev.astro.34.1.35.

Gosling, J. T., and V. J. Pizzo (1999), Formation and evolution of corotating interaction regions and their three dimensional structure, *Space Sci. Rev.*, *89*, 21–52, doi:10.1023/A:1005291711900.

Jones, G. H., A. Balogh, and R. J. Forsyth (1998), Radial heliospheric magnetic fields detected by Ulysses, *Geophys. Res. Lett.*, *25*, 3109–3112.

Jones, G. H., A. Balogh, and E. J. Smith (2003), Solar magnetic field reversal as seen at Ulysses, *Geophys. Res. Lett.*, *30*(19), 8028, doi:10.1029/2003GL017204.

Larson, D. E., et al. (1997), Using energetic electrons to probe the topology of the October 18–20, 1995, magnetic cloud, *Adv. Space Res.*, *20*, 655–658, doi:10.1016/S0273-1177(97)00453-5.

Lean, J., Y.-M. Wang, and N. R. Sheeley Jr. (2002), The effect of increasing solar activity on the Suns total and open magnetic flux during multiple cycles: Implications for solar forcing of climate, *Geophys. Res. Lett.*, *29*(24), 2224, doi:10.1029/2002GL015880.

Lockwood, M. (2001), Long-term variations in the magnetic fields of the Sun and the heliosphere: Their origin, effects and implications, *J. Geophys. Res.*, *106*, 16,021–16,038.

Lockwood, M. (2002), Relationship between the near-Earth interplanetary field and the coronal source flux: Dependence on timescale, *J. Geophys. Res.*, *107*(A12), 1425, doi:10.1029/2001JA009062.

Lockwood, M. (2003), Twenty-three cycles of changing open solar magnetic flux, *J. Geophys. Res.*, *108*(A3), 1128, doi:10.1029/2002JA009431.

Lockwood, M. (2004), Solar outputs, their variations and their effects on Earth, in *The Sun, Solar Analogs and the Climate*, *Saas-Fee Adv. Course*, vol. 34, edited by I. Redi, M. Güdel, and W. Schmutz, pp. 107–304, Springer, New York.

Lockwood, M., and C. Fröhlich (2007), Recent changes in solar outputs and the global mean surface temperature, *Proc. R. Soc., Ser. A*, *463*, 2447–2460, doi:10.1098/rspa.2007.1880.

Lockwood, M., and M. Owens (2009), The accuracy of using the Ulysses result of the spatial invariance of the radial heliospheric field to compute the open solar flux, *Astrophys. J.*, *701*, 964–973, doi:10.1088/0004-637X/701/2/964.

Lockwood, M., R. Stamper, and M. N. Wild (1999a), A doubling of the Sun's coronal magnetic field during the last 100 years, *Nature*, *399*, 437–439, doi:10.1038/20867.

Lockwood, M., R. Stamper, M. N. Wild, A. Balogh, and G. Jones (1999b), Our changing Sun, *Astron. Geophys.*, *40*, 10–16.

Lockwood, M., R. B. Forsyth, A. Balogh, and D. J. McComas (2004), The accuracy of open solar flux estimates from near-Earth measurements of the interplanetary magnetic field: Analysis of the first two perihelion passes of the Ulysses spacecraft, *Ann. Geophys.*, *22*, 1395–1405.

Lockwood, M., A. P. Rouillard, I. Finch, and R. Stamper (2006), Comment on "The *IDV* index: Its derivation and use in inferring long-term variations of the interplanetary magnetic field strength" by Leif Svalgaard and Edward W. Cliver, *J. Geophys. Res.*, *111*, A09109, doi:10.1029/2006JA011640.

Lockwood, M., M. Owens, and A. P. Rouillard (2009), Excess open solar magnetic flux from satellite data: 1. Analysis of the third perihelion Ulysses pass, *J. Geophys. Res.*, *114*, A11103, doi:10.1029/2009JA014449.

Low, B. C. (2001), Coronal mass ejections, magnetic flux ropes, and solar magnetism, *J. Geophys. Res.*, *106*, 25,141–25,160, doi:10.1029/2000JA004015.

Mackay, D. H., and A. A. van Ballegooijen (2006), Models of the Large-scale corona: II. Magnetic connectivity and open flux variation, *Astrophys. J.*, *642*, 1193–1204, doi:10.1086/501043.

McComas, D. J., J. T. Gosling, and J. L. Phillips (1992), Interplanetary magnetic flux: Measurement and balance, *J. Geophys. Res.*, *97*, 171–177, doi:10.1029/91JA02370.

Owens, M. J., and N. U. Crooker (2006), Coronal mass ejections and magnetic flux build-up in the heliosphere, *J. Geophys. Res.*, *111*, A10104, doi:10.1029/2006JA011641.

Owens, M. J., and N. U. Crooker (2007), Reconciling the electron counter-streaming and dropout occurrence rates with the heliospheric flux budget, *J. Geophys. Res.*, *112*, A06106, doi:10.1029/2006JA012159.

Owens, M. J., N. A. Schwadron, N. U. Crooker, W. J. Hughes, and H. E. Spence (2007), Role of coronal mass ejections in the heliospheric Hale cycle, *Geophys. Res. Lett.*, *34*, L06104, doi:10.1029/2006GL028795.

Owens, M. J., C. N. Arge, N. U. Crooker, N. A. Schwadron, and T. S. Horbury (2008a), Estimating total heliospheric magnetic flux from single-point in situ measurements, *J. Geophys. Res.*, *113*, A12103, doi:10.1029/2008JA013677.

Owens, M. J., N. U. Crooker, N. A. Schwadron, T. S. Horbury, S. Yashiro, H. Xie, O. C. St. Cyr, and N. Gopalswamy (2008b), Conservation of open solar magnetic flux and the floor in the heliospheric magnetic field, *Geophys. Res. Lett.*, *35*, L20108, doi:10.1029/2008GL035813.

Owens, M. J., N. U. Crooker, and N. A. Schwadron (2008c), Suprathermal electron evolution in a Parker spiral magnetic field, *J. Geophys. Res.*, *113*, A11104, doi:10.1029/2008JA013294.

Riley, P., and J. T. Gosling (2007), On the origin of near-radial magnetic fields in the heliosphere: Numerical simulations, *J. Geophys. Res.*, *112*, A06115, doi:10.1029/2006JA012210.

Rouillard, A. P., M. Lockwood, and I. Finch (2007), Centennial changes in the solar wind speed and in the open solar flux, *J. Geophys. Res.*, *112*, A05103, doi:10.1029/2006JA012130.

Schatten, K. H. (1999), Models for coronal and interplanetary magnetic fields: A critical commentary, in *Sun–Earth Plasma Connections*, *Geophys. Monogr. Ser.*, vol. 109, edited by J. L. Burch, R. L. Caravillano, and S. K. Antiochos, pp. 129–142, AGU, Washington, D. C.

Schatten, K. H., J. M. Wilcox, and N. F. Ness (1969), A model of interplanetary and coronal magnetic fields, PFSS method, *Sol. Phys.*, *6*, 442–455, doi:10.1007/BF00146478.

Schrijver, C. J., M. L. DeRosa, and A. M. Title (2002), What is missing from our understanding of long-term solar and heliospheric activity?, *Astrophys. J.*, *577*, 1006–1012, doi:10.1086/342247.

Schwadron, N. A., M. Owens, and N. U. Crooker (2008), The heliospheric magnetic field over the hale cycle, *Astrophys. Space Sci.*, *4*, 19–26 (available at www.astrophys-space-sci-trans.net/4/19/2008/).

Solanki, S. K., M. Schüssler, and M. Fligge (2000), Secular evolution of the Suns magnetic field since the Maunder minimum, *Nature*, *408*, 445–446, doi:10.1038/35044027.

Solanki, S. K., M. Schüssler, and M. Fligge (2002), Secular evolution of the Sun's magnetic flux, *Astron. Astrophys.*, *383*, 706–712, doi:10.1051/0004-6361:20011790.

Svalgaard, L., and E. W. Cliver (2005), The *IDV* index: Its derivation and use in inferring long-term variations of the interplanetary magnetic field strength, *J. Geophys. Res.*, *110*, A12103, doi:10.1029/2005JA011203.

Svalgaard, L., and E. W. Cliver (2007), A floor in the solar wind magnetic field, *Astrophys. J.*, *661*, L203–L206, doi:10.1086/518786.

Svalgaard, L., T. L. Duvall Jr., and P. H. Scherrer (1978), The strength of the Sun's polar fields, *Sol. Phys.*, *58*, 225–239, doi:10.1007/BF00157268.

Svalgaard, L., E. W. Cliver, and P. Le Sager (2003), No doubling of the Sun's coronal magnetic field during the last 100 years, *Geophys. Res. Abstr.*, *5*, 07616. (Available at http://www.cosis.net/abstracts/EAE03/07616/EAE03-J-07616.pdf)

Svalgaard, L., E. W. Cliver, and P. Le Sager (2004), IHV, a new geomagnetic index, *Adv. Space Res.*, *34*, 436–439, doi:10.1016/j.asr.2003.01.029.

Ulrich, R. K. (1992), Analysis of magnetic fluxtubes on the solar surface from observations at Mt. Wilson of A5250; A5233, in *Cool Stars, Stellar Systems, and the Sun: 11th Cambridge Workshop*, *Astron. Soc. of the Pac. Conf. Ser.*, vol. 26, edited by M. S. Giampapa and J. A. Bookbinder, pp. 265–267, San Francisco, Calif.

Wang, Y.-M., and N. R. Sheeley Jr. (1995), Solar implications of Ulysses interplanetary field measurements, *Astrophys. J.*, *447*, L143–L146, doi:10.1086/309578.

Wang, Y.-M., and N. R. Sheeley Jr. (2003), On the topological evolution of the coronal magnetic ?eld during the solar cycle, *Astrophys. J.*, *599*, 1404–1417, doi:10.1086/379348.

Wang, Y.-M., J. Lean, and N. R. Sheeley Jr. (2000), The long-term evolution of the Sun's open magnetic flux, *Geophys. Res. Lett.*, *27*, 505–508, doi:10.1029/1999GL010744.

Wang, Y.-M., J. Lean, and N. R. Sheeley Jr. (2005), Modeling the Sun's magnetic field and irradiance since 1713, *Astrophys. J.*, *625*, 522–538, doi:10.1086/429689.

M. Lockwood and A. P. Rouillard, Space Environment Physics, School of Physics and Astronomy, Southampton University, Southampton SO17 1BJ, UK. (m.lockwood@rl.ac.uk)

M. Owens, Space and Atmospheric Physics Group, Blackett Laboratory, Imperial College London, Prince Consort Road, London SW7 2BZ, UK.